

University of Montana

ScholarWorks at University of Montana

Water Topos: A 3-D Trend Surface Approach to
Viewing and Teaching Aqueous Equilibrium
Chemistry

Open Educational Resources (OER)

2-2021

Chapter 1.3: 3-D Topo Surface Visualization of Acid-Base Species Distributions: Corner Buttes, Corner Pits, Curving Ridge Crests and Dilution Plains

Garon C. Smith
University of Montana, Missoula

Md Mainul Hossain
North South University, Bangladesh

Follow this and additional works at: <https://scholarworks.umt.edu/topos>

 Part of the [Chemistry Commons](#)

Let us know how access to this document benefits you.

Recommended Citation

Smith, Garon C. and Hossain, Md Mainul, "Chapter 1.3: 3-D Topo Surface Visualization of Acid-Base Species Distributions: Corner Buttes, Corner Pits, Curving Ridge Crests and Dilution Plains" (2021). *Water Topos: A 3-D Trend Surface Approach to Viewing and Teaching Aqueous Equilibrium Chemistry*. 4. <https://scholarworks.umt.edu/topos/4>

This Book is brought to you for free and open access by the Open Educational Resources (OER) at ScholarWorks at University of Montana. It has been accepted for inclusion in Water Topos: A 3-D Trend Surface Approach to Viewing and Teaching Aqueous Equilibrium Chemistry by an authorized administrator of ScholarWorks at University of Montana. For more information, please contact scholarworks@mso.umt.edu.

Chapter 1.3

3-D Topo Surface Visualization of Acid-Base Species Distributions: Corner Buttes, Corner Pits, Curving Ridge Crests and Dilution Plains

Garon C. Smith¹ and Md Mainul Hossain²

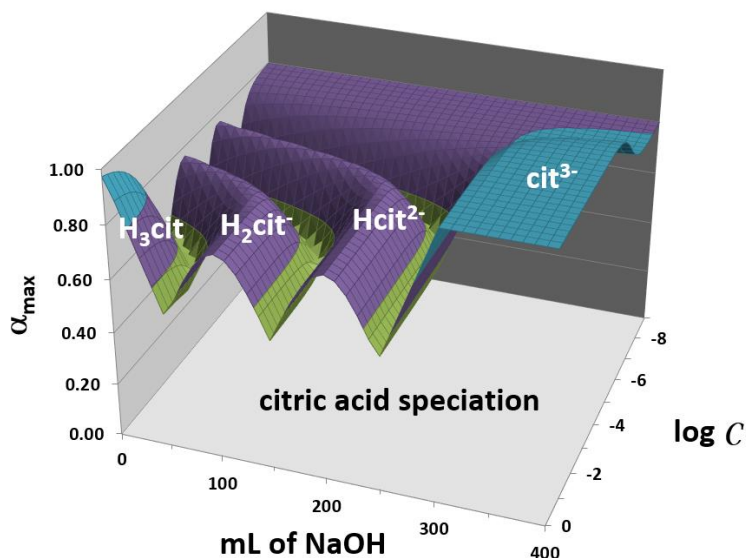
¹Department of Chemistry and Biochemistry, University of Montana, Missoula, MT 59812, ²Department of Biochemistry and Microbiology, North South University, Dhaka 1229, Bangladesh

Abstract

Species TOPOS, a downloadable software package, adds 3-D species distribution topos to earlier surfaces that showed pH (Chapter 1.1) and buffer capacity behavior (Chapter 1.2) during titration and dilution procedures. It constructs trend surfaces by plotting computed alpha distribution coefficients above a composition grid with “mL of NaOH” as the x -axis and overall system dilution ($\log C$) as the y -axis. The systematic shift from protonated to deprotonated forms is clearly visualized on a linear z -axis. Because pH and buffer capacity surfaces accompany the species topos, it is easy to see their interrelationships. On the basis of their graphical appearance, features on species topo surfaces have been named corner buttes, corner pits, curving ridge crests curving canyons and dilution plains. Ramps connecting surface features are linear when tied to additions of NaOH and logarithmic when followed on the $\log C$ dilution axis. The amphiprotic behavior of water is demonstrated through dilution procedures. Systems examined include acetic acid, CH_3COOH (a weak monoprotic acid); carbonic acid, H_2CO_3 (a weak diprotic acid), and phosphoric acid, H_3PO_4 (a weak triprotic acid). For comparative purposes, species topos are depicted for a set of three acids with hypothetical $\text{p}K_a$ s of 4.0, 7.0, and 10.0. Supplementary files include the Species TOPOS software, a macro-enabled Excel workbook that quickly generates pH, buffer capacity and alpha surfaces for any mono-, di-, or triprotic acid desired. Only the acid dissociation constants, the K_a values, are needed as inputs. Also included are a set of PowerPoint lecture slides and a document “Teaching with Species TOPOS” with sections for lecture, practice exercises, and suggested laboratory activities for introductory college courses and

upper-division or graduate courses in analytical chemistry, biochemistry and geochemistry.

Predominant species topo for citric acid



1.3.1 Introduction

Compounds with acid-base characteristics go through various protonated and deprotonated forms as solution conditions change. The fraction of a particular species is usually termed an alpha distribution coefficient, α_x , whose subscript indicates how many protons have been lost. The fraction with all protons still in place is α_0 . As an acid sample undergoes a titration with strong base, *e.g.*, NaOH, or gets diluted, protons start being stripped off. If sufficient base is added to a system, the compound ends up with no reactive protons left. Thus, α_3 in a triprotic system corresponds to the fraction in the fully deprotonated form. Standard equations for the calculation of alphas as a function of pH are well known in the literature and part of every junior-level analytical chemistry course.¹ The formula for α_0 in a monoprotic system, for instance, is given by eq 1.3-1:

$$\alpha_0 = \frac{[HA]}{[HA] + [A^-]} = \frac{[H_3O^+]}{[H_3O^+] + K_a} \quad (1.3-1)$$

The exact equations for monoprotic, diprotic and triprotic systems are included as a downloadable supplementary file as well as in a tab in the Species TOPOS workbook.

While the variation of alpha coefficients with respect to pH has been extensively discussed in the literature, this chapter describes a new dimension of species distribution behavior that accompanies dilution procedures. Because dilution affects pH, it will also change the ratio among possible species. Dilution will eventually drive speciation to the alpha values that correspond to the pH of the diluent. Examples in this paper are for diluent water at pH 7.00. Natural waters, however, will display other values depending on local geology – higher pHs with limestone bedrock and lower pHs when acid mine drainage is present.² When plotted above an underlying composition grid, alpha behaviors fall into features that appear on the accompanying topo surfaces as “corner buttes”, “corner pits”, “curving ridge crests”, “curving canyons” and “dilution plains”.

It is important to know exactly what form of a compound predominates under a given set of conditions. Some species are positively charged, some are uncharged, and some are negatively charged. Behavior in physiological and geochemical settings hinges upon which species predominates. This chapter provides topo trend surfaces from which to visualize how acid-base speciation behaves when a system undergoes alterations from the addition of a strong base or is diluted with water. Students majoring in chemistry³⁻⁵, biochemistry⁶⁻⁷ and geochemistry⁸⁻⁹ need to understand species distribution behavior. For example, it is important in biochemistry to know the form that an amino acid adopts at physiological pHs such that it can bind with a t-RNA molecule for assembly into a protein.¹⁰ This usually occurs under fairly dilute conditions. In geochemistry it is important to know under what aqueous conditions H₂S will be present in an uncharged form and partition into the air via volatilization.¹¹ Again, this occurs in fairly dilute solutions, typically parts per billion. While the main controlling factor is the pH of these systems, it is good to be able to predict how dilution can create additional species shifts.

Two earlier chapters are aimed at generating 3-D topo surfaces for acid-base systems above the same composition grid used here.^{12, 13} Chapter 1.1 characterizes a system's pH behavior while Chapter 1.2 provides details on buffer capacity. In this chapter additional sets of 3-D topos illustrate how species

distributions systematically change with solution composition. The downloadable Species TOPOS Excel workbook connects pH changes, the associated buffer capacity at each point and how much of each form of acid-base compound will be present. The Species TOPOS software incorporates all features of the two previous chapters, *i.e.*, pH and buffer capacity surfaces, plus a variety of species distribution diagrams (2-D) and species topo surfaces (3-D). The overall software package should help interested readers, especially beginning students, see the interrelationship between 1) the pH that a buffering agent establishes, 2) the buffer capacity it possesses, and 3) which conjugate acid-base pair is involved in its maintenance. At the same time, it provides insights into acid-base behavior for more advanced students. Instructors and students in upper-division and graduate-level analytical, biochemistry, aquatic chemistry, and geochemistry courses will find that the workbook contains data arrays with detailed quantitative results for every grid point. Predominant species surfaces will allow them to predict acid-base behavior trends without the need for extensive additional computations.

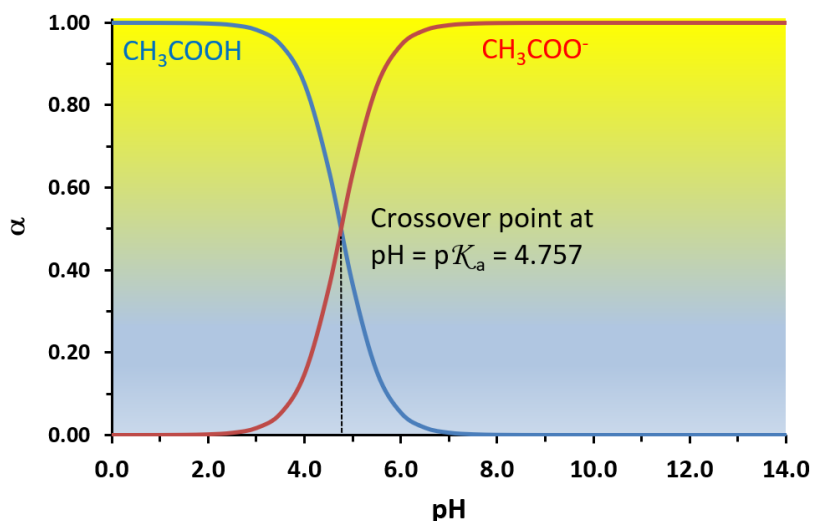
Species distribution diagrams are not new. They have been included in most treatments of acid-base behavior in analytical chemistry courses ever since the concept of pH was introduced by Sørensen in 1909.¹⁴ Seminal papers in describing graphical presentation of species distribution are attributable to Sillen.^{15,16} Calculation procedures for generating species distribution plots have been available for years, commonly presented as distributions vs. pH. Rough calculations are simple enough to do by hand, but more sophisticated numerical methods were needed to compute them more accurately. Early programs for mainframe computers appeared starting around 1958.¹⁷⁻¹⁹ With the advent of personal computers in the 1980s, computer software to calculate acid-base equilibrium properties became widely available to more general audiences. Ramette's "The Acid-Base Package" was a collection of four DOS-based programs that was featured as a *Journal of Chemical Education Software* item.²⁰ Its ALPHA program computed species values as a function of pH. In 1998 Ramette updated his earlier program to the Windows 95 environment and renamed it "Buffers Plus".²¹ This enhanced package included both styles of alpha plots – as a function of pH or as a function of the volume of titrant added. Unfortunately, these comprehensive buffer calculation software packages are no longer available. At this writing, CurTiPot, a collection of spreadsheet programs that do many of the same 2-D functions, is provided as a free download from I.G.R. Gutz.²²

1.3.2 Traditional 2-D Distribution Diagrams

Note: This section is designed to describe the traditional 2-D treatment of species distribution diagrams for readers who want more background. Those familiar with these concepts can skip to section 1.3.3.

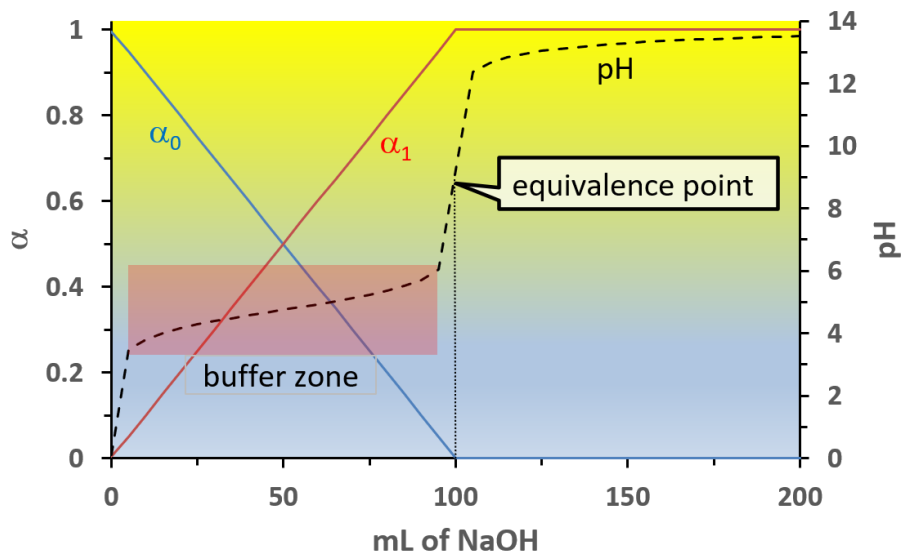
Normally, the sequential loss of protons is shown with respect to pH. Figure 1.3-1 shows the classical 2-D species distribution diagram for monoprotic acetic acid vs. pH. Its main feature is the demonstration that the crossover in the predominant form occurs when the pH is equal to the pK_a for the acid, 4.757 in this instance.

Figure 1.3-1. A traditional 2-D species distribution diagram for acetic acid, CH_3COOH .



The classical α vs. pH approach does not give a sense of the rate at which these shifts occur with addition of a titrant. Another perspective of speciation is gained by using mL of NaOH as the x -axis, just as in a titration curve. In making this change, the alphas will track species distribution shifts in exactly the way they will occur during the course of a titration. In fact, unlike the traditional alpha plots, a titration curve can be superimposed on the same figure to visualize the connection. Figure 1.3-2 shows both the alpha distribution coefficient curves PLUS the titration curve for the same monoprotic acetic acid system on a linear x -axis. Note that this is an effective way to illustrate that the buffer region, where the pH titration exhibits a plateau, occurs when you have significant amounts of both the acid and its conjugate base form present. Neither α_0 nor α_1 is 0 or 1.

Figure 1.3-2. Alpha and pH vs. mL of NaOH for 100 mL of 1.0 M acetic acid titrated with 1.0 M NaOH.



The linear nature of the alpha traces that precede the equivalence point justify the manner in which pHs are often calculated with the Henderson-Hasselbalch equation (eq 1.3-2).

$$\text{pH} \cong \text{p}K_a + \log\left(\frac{[\text{base form}]}{[\text{acid form}]}\right) \text{ or } \frac{[\text{mL NaOH}]}{[100 \text{ mL} - \text{mL NaOH}]} \text{ or } \frac{[\alpha_1]}{[\alpha_0]} \quad (1.3-2)$$

Students are coached to use the percentage of the distance to the equivalence point as the ratio of base-to-acid form in the calculation. For the example in Figure 1.3-2 with an equivalence point volume of 100 mL, the half-equivalence point volume is 50 mL. At this point, the Henderson-Hasselbalch calculation for [base form]/[acid form] could use either the volumes, (50 mL)/(100 mL – 50 mL) = 1, or the α_1/α_0 ratio, 0.500/0.500 = 1.00, to demonstrate that $\text{pH} = \text{p}K_a = 4.757$ at the crossover point between CH_3COOH and CH_3COO^- . This linear relationship between volume of NaOH and the value of the α ratio involved in the buffer zone is generally true, but systems exist for which this assumption is not valid, namely very low $\text{p}K_a$ s, very high $\text{p}K_a$ s and poorly separated sequential $\text{p}K_a$ s in polyprotic systems.

Figure 1.3-2 also illustrates that the equivalence point break signals the complete conversion of a conjugate acid-base pair; all acetic acid is transformed

to its conjugate acetate form. At 100 mL the α_1 reaches and stays essentially equal to 1. At the same point, α_0 bottoms out at essentially 0.

Logarithmic species distribution diagrams are also fairly common to find in the literature, especially with discussions of geochemistry in natural waters. Again, log alphas are traditionally plotted with pH as an x -axis (Figure 1.3-3). After the crossover point has been passed, there are no additional features seen in the α_0 trace; it simply follows a linear trend to lower and lower values. The α_1 trace is just the reverse. It rises at a constant slope and then flattens out near 0 beyond the crossover point.

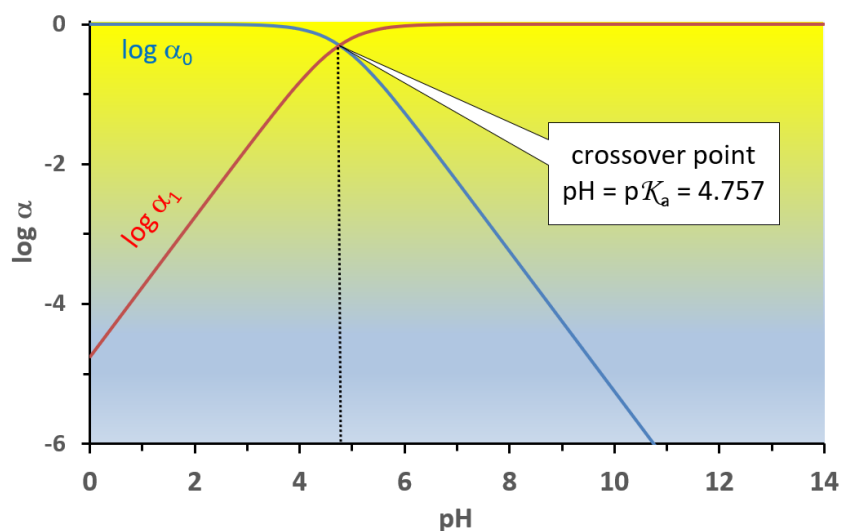
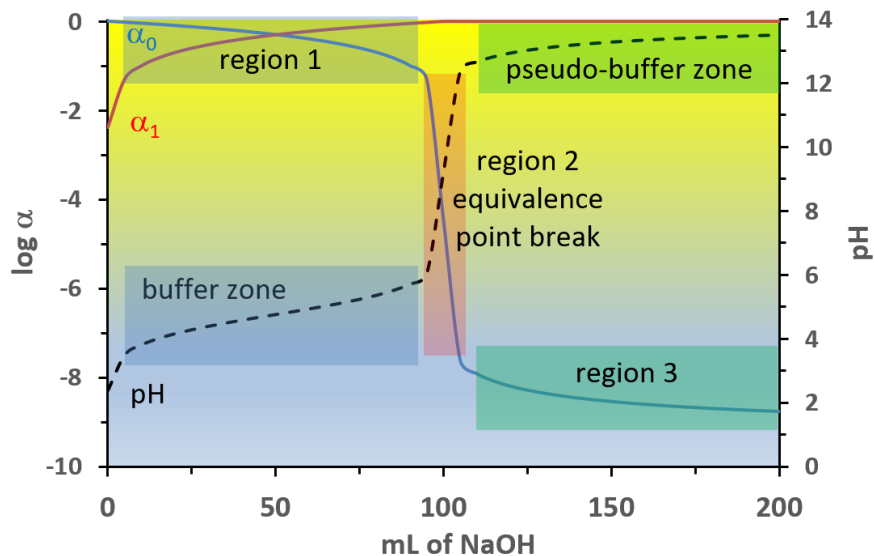


Figure 1.3-3. Traditional 2-D plot of log alpha vs. pH for acetic acid.

When the log alphas are plotted against a linear x -axis (mL of NaOH added), additional alpha behaviors are seen (Figure 1.3-4). Their significance becomes obvious when a pH titration curve is superimposed on the figure. Three regions of associated behavior are seen in the α_0 trace: 1) a shallowly descending shoulder that traverses the buffer zone; 2) a precipitous drop that mirrors the equivalence point rise on the pH titration curve; and 3) a post-equivalence pseudo-buffering zone, a slope that gradually becomes asymptotic to the $\log \alpha_0$ value of the pH 14 titrant. For acetic acid, the value of $\log \alpha_0$ at the final point on the plot is -8.77. The limiting value would ultimately be -9.24 when the system achieved a pH = 14.00. Plots of $\log \alpha_0$ vs. pH do not provide insights into this multi-regional behavior.

Figure 1.3-4. 2-D plot of log alpha and pH vs. mL of NaOH for 100.0 mL of 1.0 M acetic acid titrated with 1.0 M NaOH.



The species distribution diagrams for polyprotic acids contain multiples of the same sorts of features. Carbonic acid, H_2CO_3 , illustrates this nicely. Figure 1.3-5 presents the linear alphas. The linear plot of alpha vs. pH (Panel a) gives the familiar diprotic acid pattern of an α_1 -peak centered between shoulders for α_0 and α_2 on either side. The linear plot of alpha vs. mL of NaOH (Panel b) shows X-shaped crossovers for each of the two buffer zones followed by flat pseudo-buffer traces that eventually flatten at 1.00 for α_2 and at 0.00 for both α_0 and α_1 . The crossovers clearly illustrate the systematic conversion of conjugate acids into their conjugate bases as the two, successive equivalence points are approached.

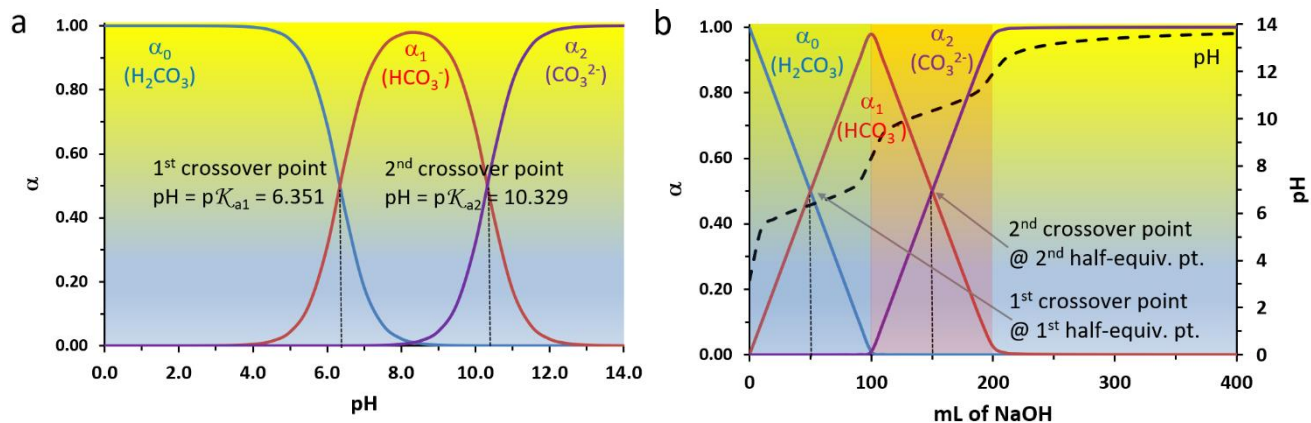


Figure 1.3-5. Linear 2-D species distribution diagrams for 100 mL of a 1.0 M solution of carbonic acid. a) α vs. pH; b) α vs. volume. (Shading in Panel b indicates titration of first and second protons.)

The logarithmic plots of alpha for the two styles of x -axes are displayed as Figure 1.3-6. Plotted against a pH x -axis (Panel a), $\log \alpha$ traces show nice crossover points but only a subtle bend in the slope at the equivalence points. On the other hand, plotted against mL of NaOH (Panel b), there are prominent crossover points as well as dramatic shifts in speciation at each equivalence point break. Because a pH curve can be superimposed on this diagram, the close tie between it and the shift in species should help students better understand what is going on at any point in the process.

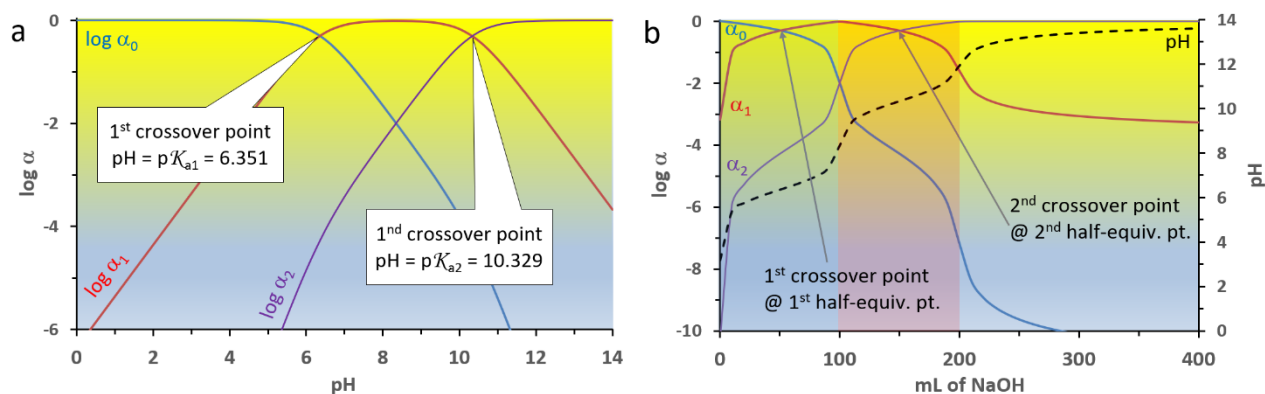


Figure 1.3-6. Logarithmic 2-D species distribution diagrams for 100 mL of a 1.0 M solution of carbonic acid. a) α vs. pH; b) α vs. volume. (Shading in Panel b indicates titration of first and second protons.)

1.3.3 Three-Dimensional Species Distribution Diagrams

Both addition of base and dilution to an acid solution can change the pH and, hence, the distribution of species. A 3-dimensional species distribution diagram permits simultaneous visualization of shifts caused by both of these variables. Our composition grid is established with “mL of NaOH” on the x -axis (as for a typical titration of an acid sample) and overall dilution of the system ($\log C$) on the y -axis. Plotted above this grid on the z -axis are the alpha distribution coefficients associated with the underlying pair of composition grid coordinates. The resulting 3-D surface topos depict how the two grid variables affect the relative amount of each species – which one is predominant and which ones are essentially insignificant. The computer program entitled Species TOPOS is a collection of Visual Basic macros embedded within an Excel workbook. It is provided as a downloadable supplementary file through which the reader can

modify K_a values to represent any desired mono-, di- or triprotic acid system. It also includes the computational routines that generate the companion pH and buffer capacity topos. As such, it is an overall software package that provides three types of topo surfaces – pH, buffer capacity and species distributions. Values for the K_a 's of the sample systems included in this chapter are taken from Martell and Smith's *Critical Stability Constants*.²³

The calculations displayed in this paper assume that the analyte is a 100-mL aliquot of acid. For the dilution axis, both the acid analyte and the NaOH titrant are assigned identical concentrations. Thus, equivalence points always occur at 100-mL intervals. With a monoprotic acid, for example, the x -axis ranges in 5.00-mL steps from 0 to 200 mL, terminating 100 mL beyond the equivalence point. The y -axis is logarithmic and provides the starting concentration for both the analyte and titrant, $\log C_a$ and $\log C_b$. These values begin at 0 (1 M) and are reduced in -0.25 log-unit increments until a log concentration of -9 (1×10^{-9} M) is reached. The two axes establish a composition base that is $41 \times 37 = 1517$ total grid points.

At each grid point, a polynomial equation is solved with an iterative procedure for the concentration of H_3O^+ to 16 significant figures. The polynomial forms used for strong acids, monoprotic acids, diprotic acids and triprotic acids are widely available.⁵ The $[H_3O^+]$ is simply converted to a pH value to create the pH titration surface. Computation of the associated pH and buffer capacity surfaces was discussed in detail in Chapters 1.1 and 1.2.^{12,13} The subsequent calculations necessary for producing the species topo surfaces are trivial; one simply substitutes the $[H_3O^+]$ value for a grid point into the traditional alpha coefficient formulas. The novelty here is the added dilution dimension for speciation shifts. Traditional alpha vs. pH plots cannot address dilution-caused shifts in equilibrium.

The α_0 topo for HA, the undissociated form of a weak monoprotic acid, can have different appearances dependent on the value of the pK_a (Figure 1.3-7). If the pK_a is small, the only feature is a pointed butte at the left corner of the surface as plotted. The butte grows in height and begins to show a rounded top near a pK_a of 4 (Panel a). The butte stretches in the dilution direction with increasing pK_a values. At $pK_a = 6$, the dilution plain at the back begins to rise and a front corner pit begins to form. By $pK_a = 7$, the dilution plain is at a half-way

alpha value of 0.5 (Panel b). At $pK_a = 8$ the dilution plain is 90% of the way to the top. At $pK_a = 10$ (Panel c) the floor of the front corner pit becomes narrower. Connections from the top of the butte in the mL of NaOH direction are always linear and hit a value nearly 0.00 at the 100-mL mark. Connections of the corner butte or corner pit to the dilution plain are logarithmic in character. A PowerPoint “movie” visualizing α_0 surfaces for unit steps in pK_a from 0 to 14 is found as part of the downloadable PowerPoint lecture that is a supplementary file for this chapter.

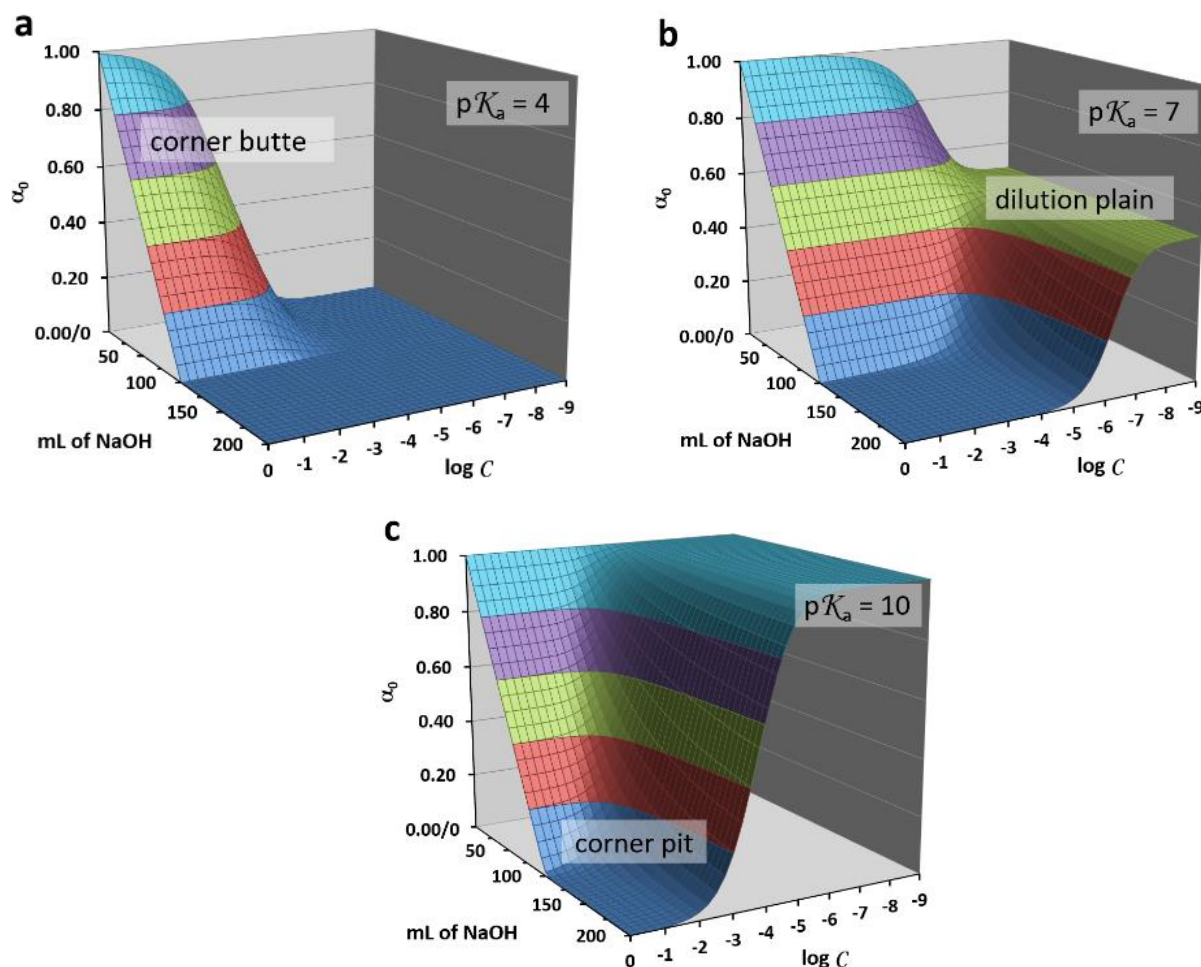


Figure 1.3-7. The α_0 surfaces for three hypothetical monoprotic acids with pK_a s of 4, 7 and 10.

Note that all surfaces show the same linear ramp feature on the left edge, a manifestation of the linear change in speciation during the titration procedure. The equivalence point occurs at a volume of 100 mL, the location of the ramp’s

lower edge. The morphologies of the three surface types in Figure 1 are based on the diluent water having a pH of 7.

These surfaces visually reveal that diluent water can act as a base in some cases but not in others. Looking at the back edges of the Figure 1.3-7 surfaces (the 0.0-mL slice), one sees that diluent water acts as a base, stripping protons off the acids that have pK_a s of 4 and 7. Loss of protons is indicated by the dropping α_0 values in the dilution direction of Panels a and b, similar to the way they would appear during a titration procedure. For the pK_a 4 acid, the α_0 goes from almost 1.0 to near 0.0 as dilution drives the pH toward 7. For the pK_a 7 acid, the α_0 moves from almost 1.0 to about 0.50 as it is diluted. Diluent water has little effect for the pK_a 10 acid; the α_0 value of the 0.0-mL slice of Panel c shows no visible change because the pK_a value is well above the diluent water's pH of 7. The first proton is untouched at pH 7.

Panels b and c of Figure 1.3-7 illustrate that diluent water can also act as an acid, donating protons to A^- . The front edges of these two panels, the 200-mL slice, illustrate logarithmic curves that raise α_0 values as dilution proceeds. The pK_a 10 acid system goes through a full logarithmic sigmoid curve as α_0 goes from near 0.0 to near 1.0. The pK_a 7 acid system goes halfway, starts near 0.0 and stabilizes at 0.50.

The α_1 topos for A^- (Figure 1.3-8), the deprotonated form of a monoprotic acid, are the complements to the α_0 surfaces. Where the α_0 surface is high, the α_1 surface will be low and *vice versa*. For comparative purposes the viewing angle is maintained, even though it forces the viewer to look at the underside of the surface in some regions. The appearance of α_1 surfaces is also dependent on the pK_a value of the acid involved – a corner pit for $pK_a = 4$ (Panel a), an intermediate dilution plain with ramps for $pK_a = 7$ (Panel b), and a corner butte for $pK_a = 10$ (Panel c) are illustrated here. All three display a linear ramp on the left edge that corresponds to the linear addition of base titrant. There is a complementary incidence of logarithmic S-curves as well on the front and back edges.

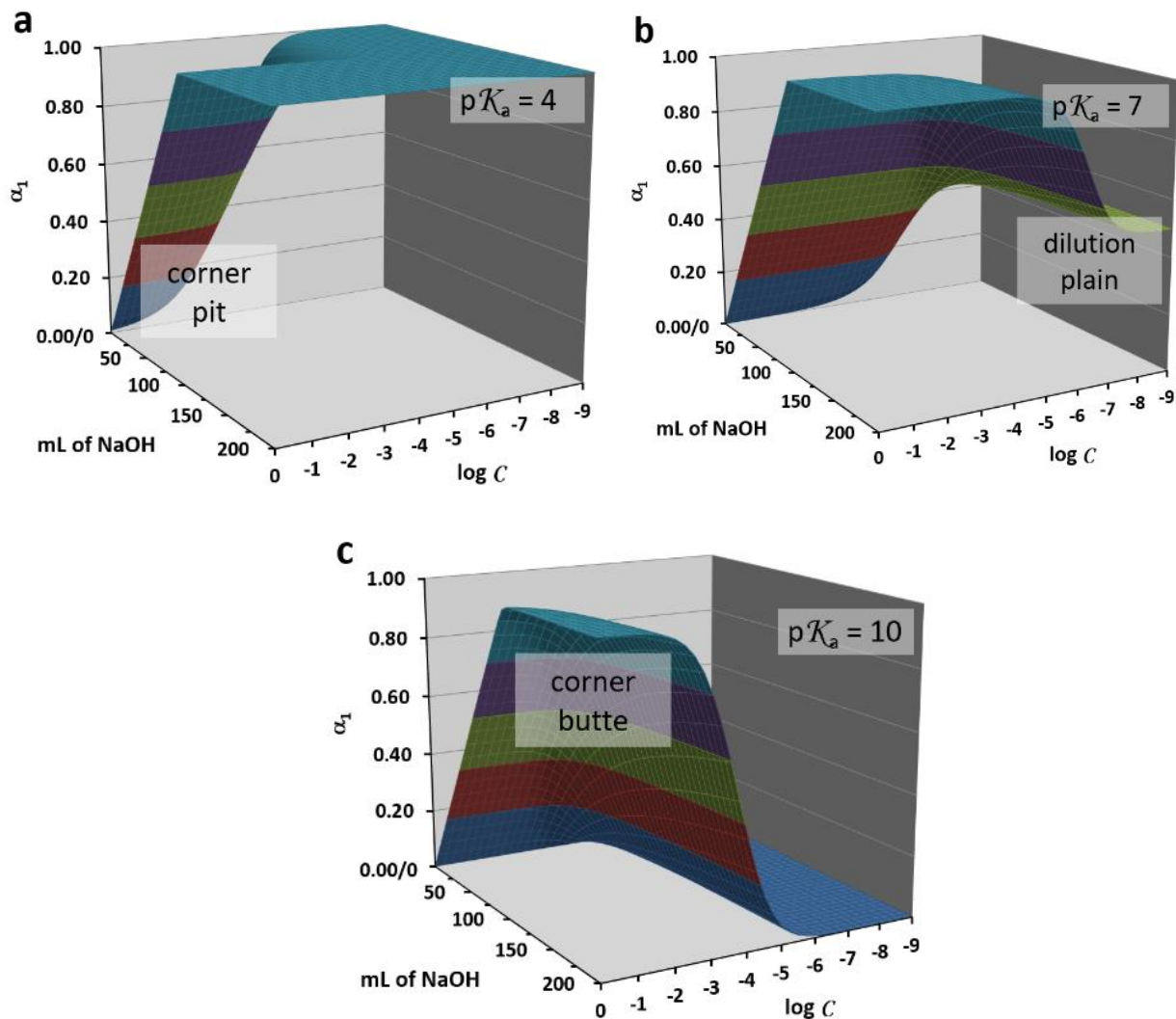


Figure 1.3-8. The α_1 surfaces for three hypothetical monoprotic acids with pK_a s of 4, 7 and 10.

Similar to how a 2-dimensional plot can summarize all species with a series of traces, a 3-dimensional predominance surface can visualize the relationships between all species in a system. These predominance surfaces simply display the largest of the alpha values at each composition grid-point. The resultant surface shows corner butte tops and the dilution plain with intervening curved canyons in most instances. For a monoprotic system there will be at most two regions, one dominated by α_0 and one by α_1 . There are two ways to plot this surface. Figure 1.3-9a is the wire-frame variety and Figure 1.3-9b is the contour map version. The wire-frame version helps one visually interpret valleys and ridges. The contour map

makes it easier to determine the exact grid-point coordinates of a feature's boundaries. A small change in viewing angle has been implemented for the wire-frame surface for optimal viewing. Solid relief shading is also used to improve feature identification. A visual artifact from the grid-point spacing causes the shading to stipple, particularly in the bottom of the contour map canyons. We have labeled the two regions for the pK_a 4 acid used to generate the figure. Figure 1.3-9 displays a curving canyon that separates the two regions. The trench runs straight backwards until dilution starts to alter the pH. This is an indication of where buffering against addition of water begins to fail.

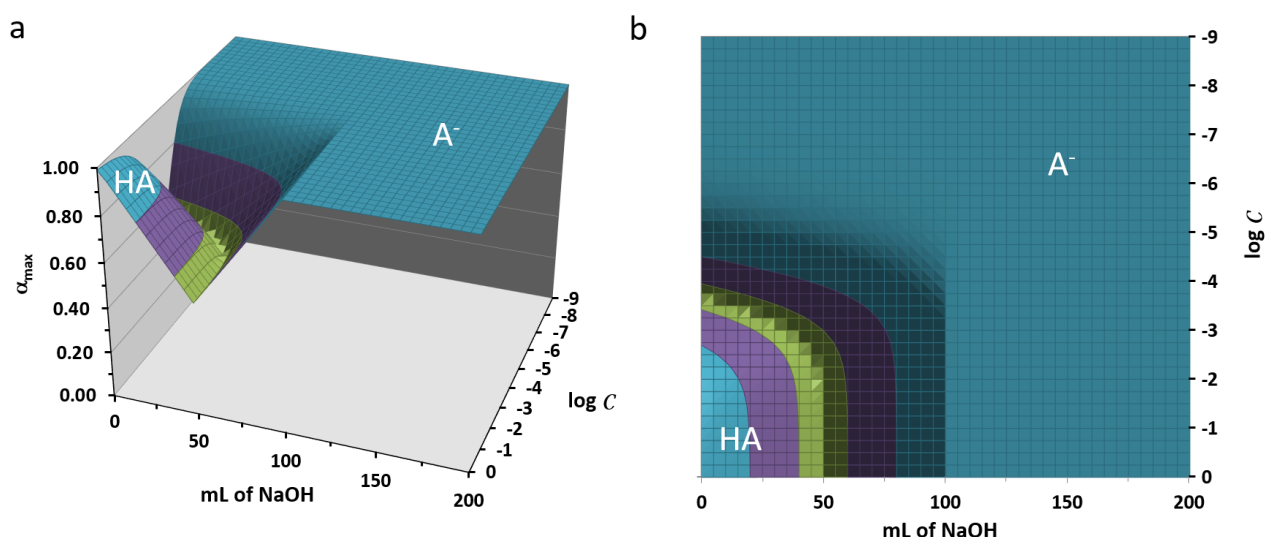


Figure 1.3-9. Predominant species surfaces for a pK_a 4 acid. a) shaded wire-frame surface; b) shaded contour map.

Log alpha topos provide insights into speciation under trace-level conditions. This is most often encountered in geochemistry applications, but it also has utility in considering biochemical species that may be present at low levels, for example amino acids or pharmaceuticals. Figure 1.3-10 holds the $\log \alpha_0$ and $\log \alpha_1$ topos for the same hypothetical monoprotic acid with a $pK_a = 4$. The character of the edges is reversed. The left edge has a logarithmic shape while the front and back edges show linear changes. The $\log \alpha_0$ surface (Panel a) looks very similar to the topo for $[H_3O^+]$ as seen in the Species TOPOS workbook pages but not included here. It is essentially a complementary topo to the pH surface and possesses the same types of surficial features – a buffer plateau, an equivalence point cliff, a post-equivalence-point pseudo-buffer ramp and a pH 7

dilution plain. The topo for $\log \alpha_1$ is a high plain with a droop at the left-hand corner in the back. Once the acid is mostly deprotonated, α_1 takes on a value that does not differ substantially from 1 which gives a $\log \alpha_1$ value near 0.

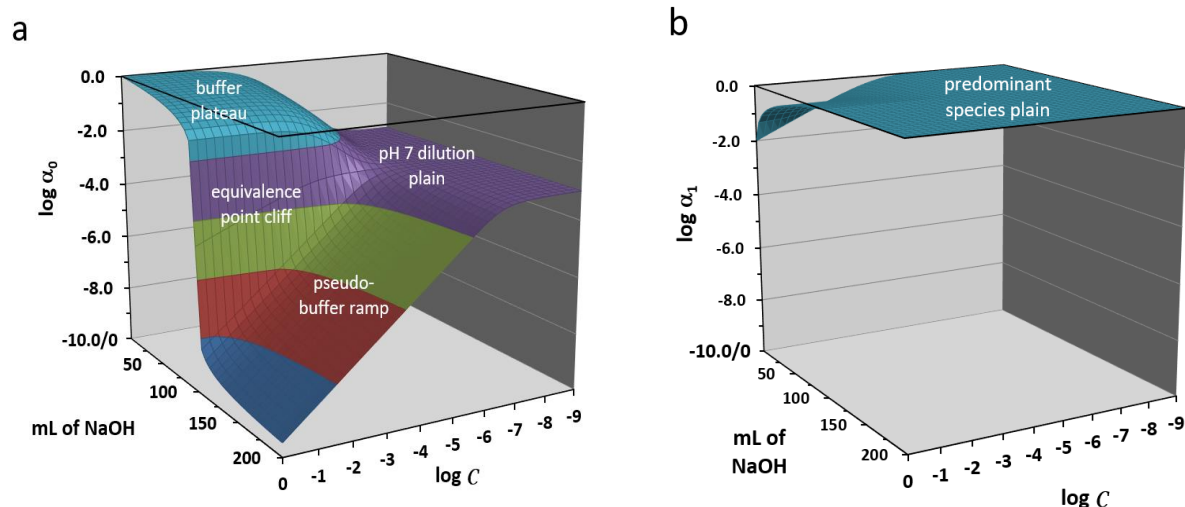


Figure 1.3-10. Log alpha plots for a hypothetical monoprotic acid with a pK_a of 4. a) $\log \alpha_0$; b) $\log \alpha_1$.

1.3.4 Species Topos for Polyprotic Systems

Polyprotic acid systems have a 3-D topo surface for each possible species. The appearance of the surface for a polyprotic acid's α_0 will not differ from that for a monoprotic acid. A similar generalization is true for the completely dissociated species; it will look like a monoprotic acid's α_1 surface. The only new type of surface will be that for intermediate species. These will give rise to "curving ridge crests". Our example systems here are carbonic acid and phosphoric acid, the two systems most responsible for buffering blood at a pH of about 7.40. The normal physiological concentrations of these two systems have a ratio for H_2CO_3/HCO_3^- of about 1.0 to 10.7 and a ratio for $H_2PO_4^-/HPO_4^{2-}$ of about 1.0 to 1.5.

Figure 1.3-11 displays the species topos for carbonic acid with $K_{a1} = 4.46 \times 10^{-7}$ and $K_{a2} = 4.69 \times 10^{-11}$. The α_0 surface (Panel a) shows a dilution plane located around 0.183 since this is the α_0 value at pH 7 that persists across the entire

volume direction of the grid. The linear consumption of H_2CO_3 appears on its left edge and its dilution-driven dissociation is seen on the back edge. The α_1 surface shows a curving ridge crest with an elevated back-side sitting at a dilution plateau elevation of 0.816, the complement of α_0 . The α_1 ridge curves to the right because the pH of the dilution water at 7 is lower than $\text{p}K_{a2}$ at 10.329. A similar effect happens on the other side of the α_1 ridge but is not visible in the viewing angle of Panel b. The α_2 surface is a corner butte. It displays a linear formation of CO_3^{2-} from HCO_3^- on its left edge. The right-front edge is a logarithmic curve caused by the pH 7 diluent protonating CO_3^{2-} .

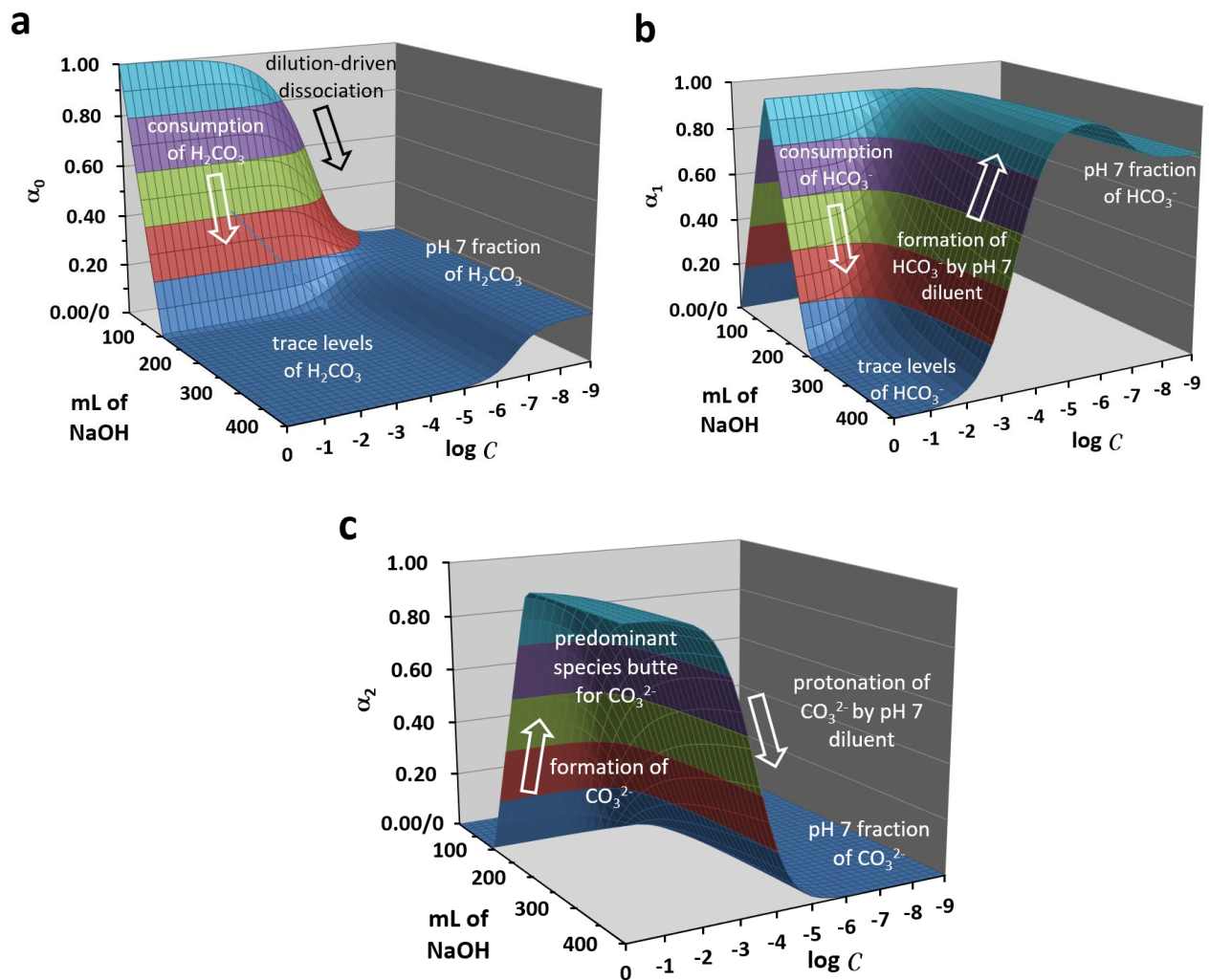


Figure 1.3-11. Linear species top surfaces for the carbonic acid system.
a) α_0 (H_2CO_3); b) α_1 (HCO_3^-); c) α_2 (CO_3^{2-}).

The best view of the interplay between all possible species can be seen with the predominant species topos (Figure 1.3-12). The wire-frame version (Panel a) makes it clear which features are ridges and which features are valleys. The contour map version (Panel b) clearly shows the complete extent of the curving canyons to either side of the α_1 ridge. The curves result during a dilution procedure when either H_2CO_3 or CO_3^{2-} is predominant. The diluent water at pH 7.0 acts as a titrant in either case. Because $\text{p}K_{a1}$ (6.352) is slightly lower than 7.0, the water acts as a base to deprotonate H_2CO_3 , reaching a crossover point around 10^{-6} M on the $\log C$ axis. A comparable process happens when CO_3^{2-} is the predominant form. Here, the water at pH 7.0 is much lower than $\text{p}K_{a2}$ (10.329), so the water acts as an acid and protonates CO_3^{2-} . The difference between $\text{p}K_{a2}$ and 7.0 is quite large, so the crossover point occurs just below 10^{-3} M on the $\log C$ axis. The predominant species in the dilution plain region is HCO_3^- . For this reason, the predominance surface shows an HCO_3^- shelf at the back. Dashed lines for equivalence point volumes of 100 and 200 mL are included in the figure for reference. This demonstrates that equivalence points are only relevant under fairly concentrated conditions. Their importance is eventually decreased by the influence of the diluent's pH. The stippling at the bottom of the contour trenches, as mentioned above, is an artifact of our gridded data. This also creates the wrinkling in the wire-frame surface's bottom side.

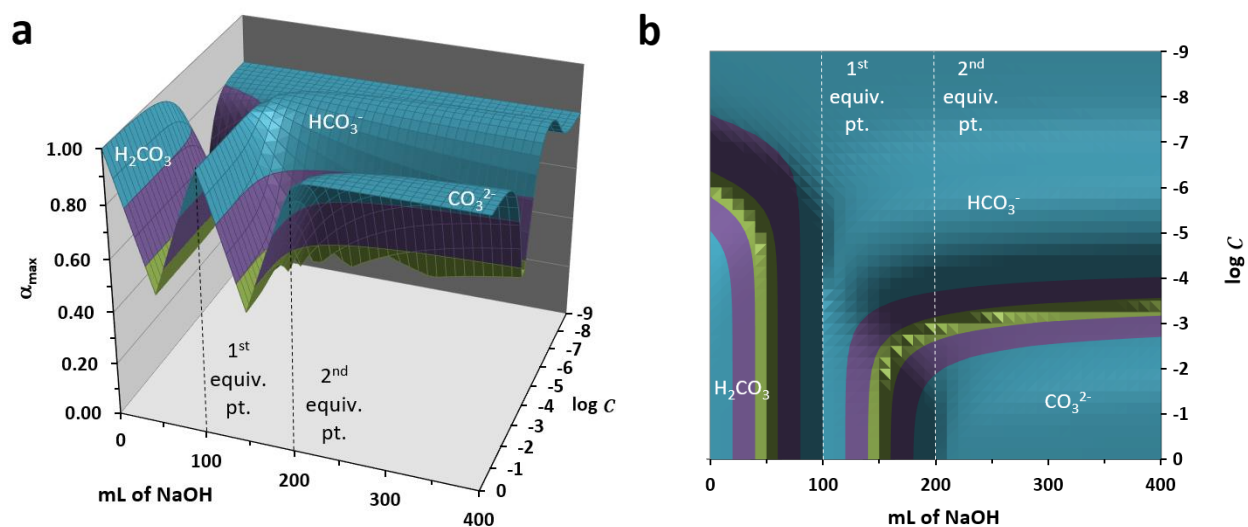


Figure 1.3-12. Predominant species surfaces for the carbonic acid system. a) shaded contour map; b) shaded wire-frame surface.

The $\log \alpha$ species tops for carbonic acid are seen in Figure 1.3-13. Each equivalence point in a system with well separated K_a s has an associated cliff feature on the $\log \alpha_0$ surface (Panel a), a first cliff at 100 mL and a second cliff at 200 mL of NaOH for the carbonic acid $\log \alpha_0$ topo seen here. A linear dilution ramp leads upwards from the low spot in the front corner pit. Finally, a dilution plain is seen as one moves to lower $\log C$ values. In between the two cliffs is a small shoulder representing a buffer plateau region for the $\text{HCO}_3^-/\text{CO}_3^{2-}$ conjugate acid-base pair. The $\log \alpha_1$ topo's main feature is the ridge crest standing out between the two equivalence point cliffs. The $\log \alpha_2$ topo is somewhat complementary to the $\log \alpha_0$ topo.

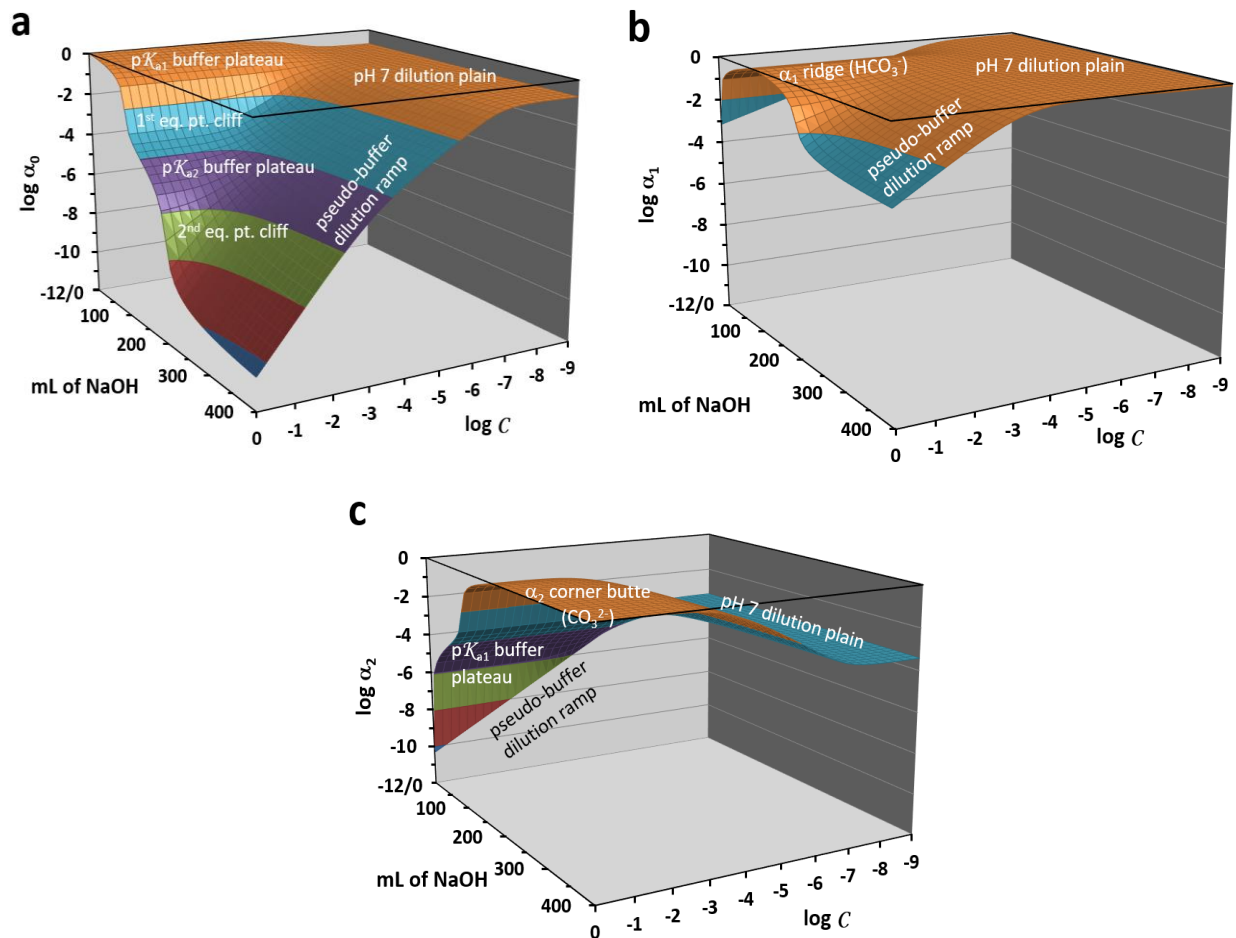


Figure 1.3-13. Log α tops for carbonic acid. a) $\log \alpha_0$ (H_2CO_3); b) $\log \alpha_1$ (HCO_3^-); c) $\log \alpha_2$ (CO_3^{2-}).

Finally, we present phosphoric acid as an example triprotic system. The K_a s are 7.11×10^{-3} , 6.34×10^{-8} , and 4.22×10^{-13} . These yield pK_a s of 2.148, 7.198 and 12.375, respectively. Individual α topos are found in Figure 1.3-14. Assembling the images in α -order allows the observer to see how the α_0 through α_3 surfaces contribute to the overall α_{\max} predominance diagrams. Note how small the regions of dominance are for both the H_3PO_4 and PO_4^{3-} forms. They are both corner butte surfaces. Dilution or motion along the mL of NaOH axis very quickly transforms them into $H_2PO_4^-$ and HPO_4^{2-} , respectively. Here is visual evidence that the two intermediate forms are the only ones that will exist in other than fairly

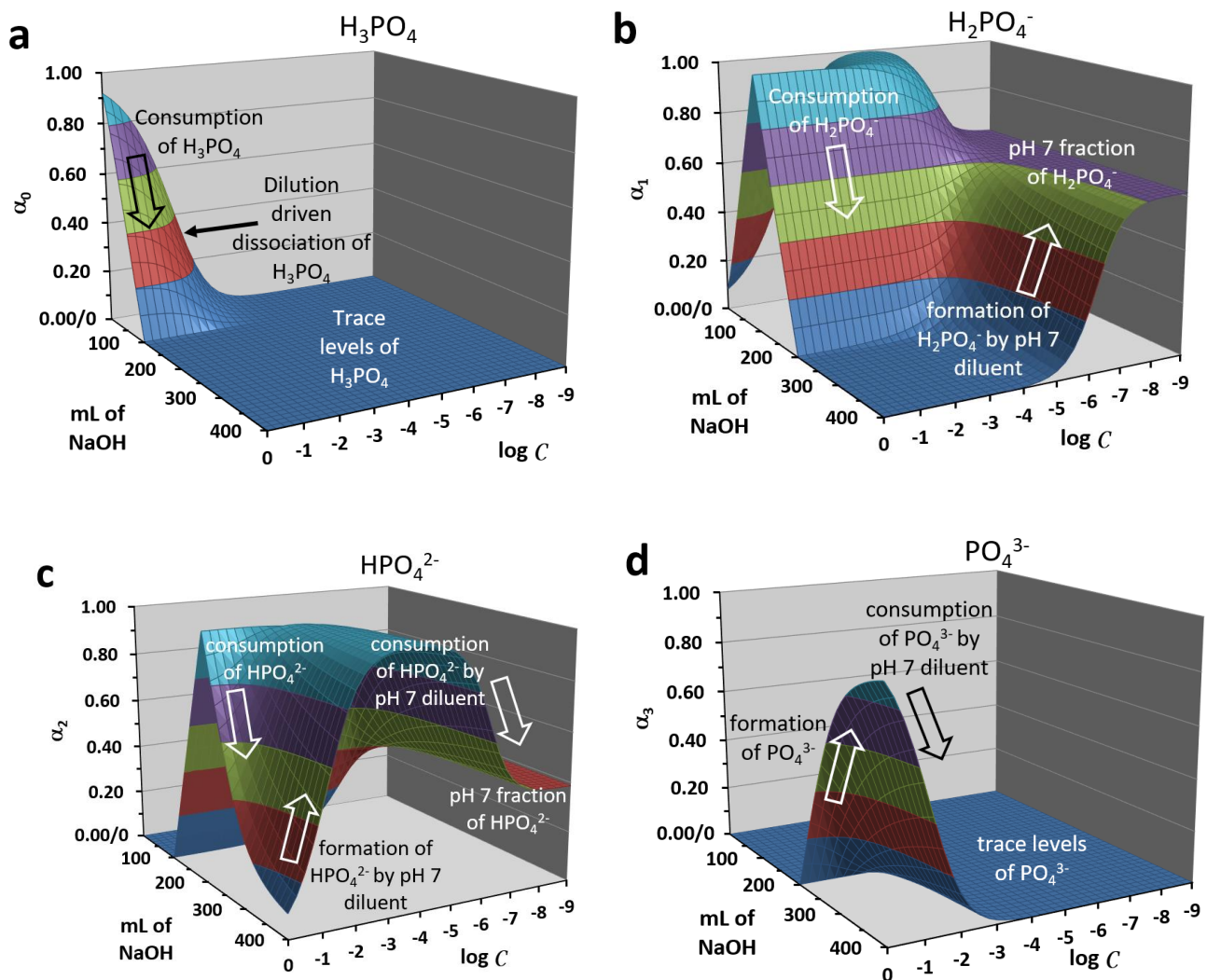


Figure 1.3-14. Species surfaces for phosphoric acid. a) α_0 (H_3PO_4); b) α_1 ($H_2PO_4^-$); α_2 (HPO_4^{2-}); α_3 (PO_4^{3-}).

concentrated solutions. Note that all left topo edges are linear in character while the front and back edges are logarithmic curves. The dilution plain reveals that H_2PO_4^- is the predominant species near pH 7 with an α_1 value of 0.614. Given that $\text{p}K_{a1}$ is less than 7 and $\text{p}K_{a2}$ is greater than 7, the ridge on the α_1 topo curves to the left and the ridge on the α_2 topo curves to the right.

The two predominant species plots are collected into Figure 1.3-15. Here is visual evidence that the H_2PO_4^- and HPO_4^{2-} forms are the only ones that will exist in other than fairly concentrated solutions. The dilution plain reveals that $\text{H}_2\text{PO}_4^{2-}$ is the predominant species near pH 7 with an α_1 value of 0.614. Its purple shelf extends across the entire composition grid at the $\log C = -9$ end. Given that $\text{p}K_{a1}$ is less than 7 while $\text{p}K_{a2}$ and $\text{p}K_{a3}$ are greater than 7, the first trench on the predominant species surface will curve to the left while the second and third trenches will curve to the right. Because $\text{p}K_{a2}$ is very close to 7, its curve occurs further back than the other two. The superimposed equivalence points lines occur where species ridges are at a maximum α -value for H_2PO_4^- and HPO_4^{2-} under concentrated conditions. The valleys represent cross-over points and fall at half-equivalence points, *i.e.*, 50-, 150- and 250-mL of NaOH.

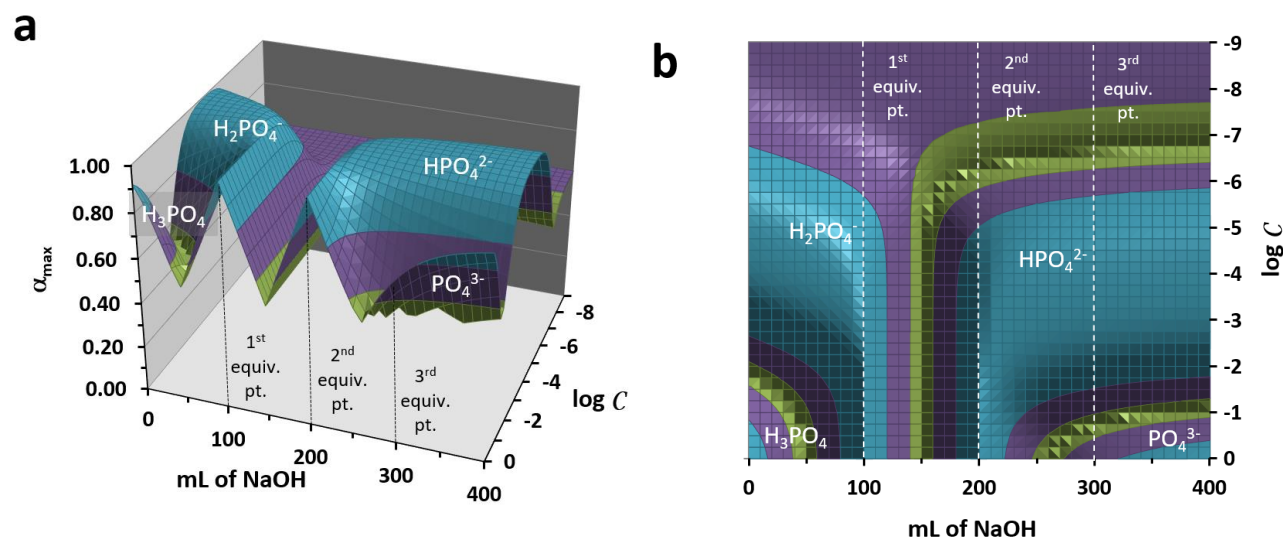


Figure 1.3-15. The predominance surfaces for the phosphoric acid. a) wire-frame; b) contour map.

The four $\log \alpha$ topos for the phosphoric acid system comprise Figure 1.3-16. These show similar features to those already described for the carbonic acid system, though several subtle points are worth discussing. Most significantly,

note that the pK_{a3} value (12.149) is not well separated from the pH of the titrant (14.0). Because of this, there are no visible cliffs at 300 mL, the third equivalence point. Viewed from the right angle, however, a slight kink in the surface can be spotted. As there are two intermediate species, the position of the ridge crest moves from 100 mL for $\log \alpha_1$ to 200 mL for $\log \alpha_2$. Lastly, note that the topo surfaces for $\log \alpha_1$ and $\log \alpha_2$ consist of a high plain covering most of the composition grid. This signifies that, under most conditions, these are the two most important species in this system, $H_2PO_4^-$ and HPO_4^{2-} . The other two species only predominate in limited ranges. H_3PO_4 requires low pH and high concentrations to prevail; PO_4^{3-} requires high pH and high concentrations to dominate.

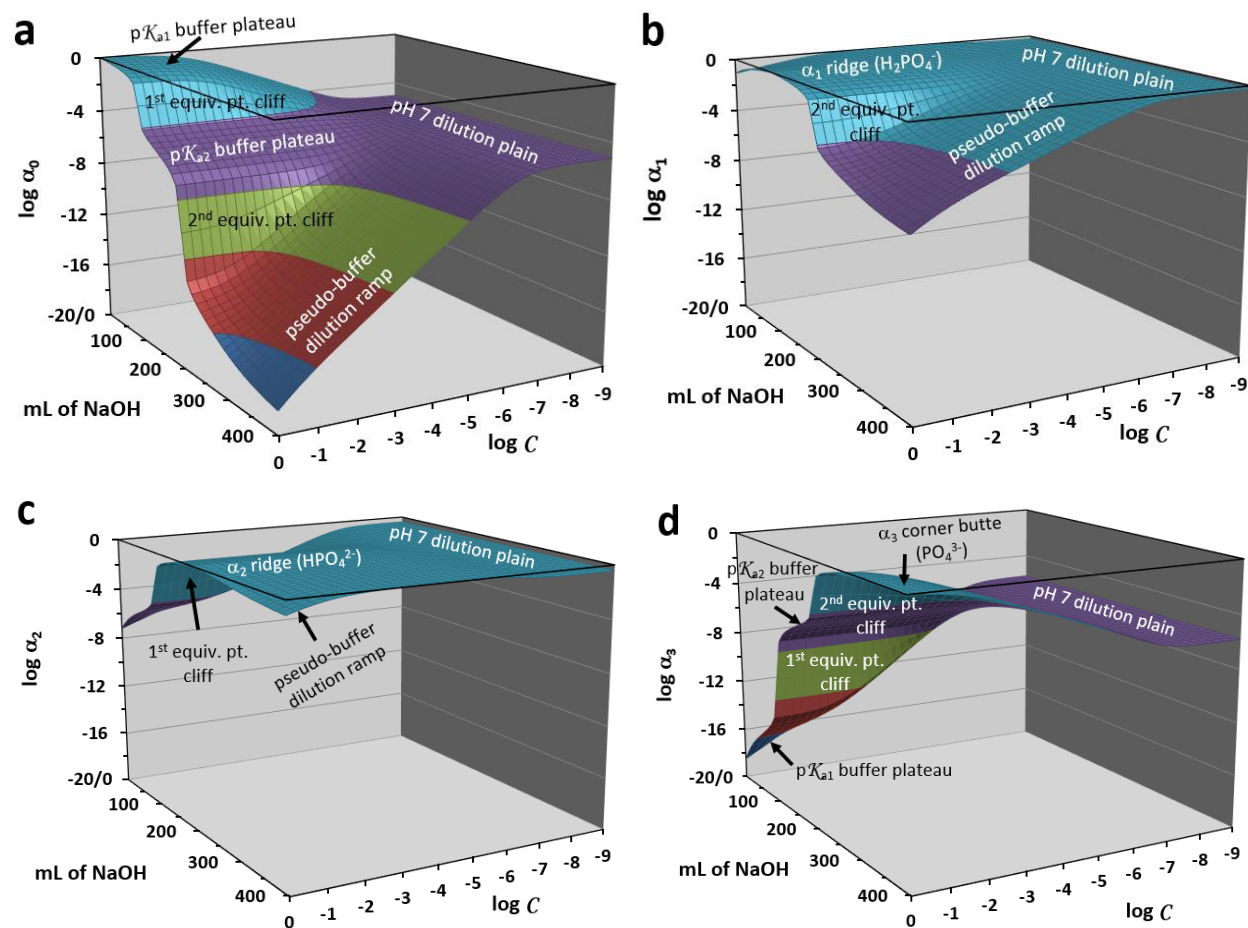


Figure 1.3-16. Log α topos for phosphoric acid. a) α_0 (H_3PO_4); b) α_1 ($H_2PO_4^-$); α_2 (HPO_4^{2-}); α_3 (PO_4^{3-}).

1.3.5 Conclusions

This chapter introduces the use of three-dimensional trend surfaces to visualize the interplay between the various protonated and deprotonated forms in which an acid can exist. Its novel aspect is a demonstration of how dilution can alter the species forms significantly. Thus, the species topographies, built above a titration/dilution composition grid, reveal a new appreciation of how shifts in protonated forms can occur. Our composition grid diagrams blend the combined effects of both pH and dilution. The pH is most strongly driven by progress on the “mL of NaOH” titration axis. But more subtle changes in pH occur with dilution. The diluent in all cases for this chapter was water at pH 7.

Species topographies show:

- The sequential loss of protons from an acid as base is added to a system;
- Predominant species surfaces that summarize the combined effects on shifts in chemical form from both mL of NaOH added and dilution;
- The amphiprotic behavior of diluent water as it acts as a base when the system pH is below 7 and as an acid when the system pH is above 7.

The Species TOPOS software can easily be used by freshman or high school students in an introductory collegiate course. An understanding of its fine points, though, will require the chemical intuition of students in junior- or graduate-level courses in analytical chemistry, biochemistry and aquatic chemistry. As was true with its predecessors, pH TOPOS (Chapter 1.1) and BufCap TOPOS (Chapter 1.2), the speed and ease with which new systems can be visualized makes this a powerful tool for simulation studies. Because it is implemented via macros in Microsoft Excel, no new software need be purchased in order to run it. It runs quickly enough (about 25 seconds) to conveniently be used for “on the fly” calculations by an instructor during a classroom session.

1.3.6 Supplementary Files

Five downloadable files are included as additional supplements for this chapter:

1. The free downloadable Species TOPOS software embedded in a Microsoft Excel workbook.
2. A Microsoft PowerPoint slide lecture with which to teach 3-D species distribution topography.
3. A “Teaching with Species TOPOS” Microsoft Word document that contains itemized teaching objectives, suggested Species TOPOS worksheet activities (homework, pre-lab, recitation or peer-led team discussions) and coordinated laboratory experiments.
4. A Microsoft Word document displaying the standard algebraic expressions for α_0 , α_1 , α_2 , and α_3 .
5. A listing of the Visual Basic code for the Species TOPOS macros that compute the $[H_3O^+]$ for each grid point.

Acknowledgements

We thank the Department of Chemistry and Biochemistry at the University of Montana for a graduate teaching assistantship that supported early phases of this research. North South University’s Department of Biochemistry and Microbiology has provided faculty support for this project. Dr. Patrick MacCarthy from the Colorado School of Mines helped develop the topographic trend surface approach in aqueous equilibrium settings. Daniel D. Barry’s assistance as an undergraduate researcher helped perform experimental verifications of computed results.

References:

1. Harris, D. *Quantitative Chemical Analysis*, 8 ed.; W.H. Freeman: New York, 2011.
2. Webb, J. A; Sasowsky, I.D. The Interaction of Acid Mine Drainage with a Carbonate Terrane: Evidence from the Obey River, North-Central Tennessee, *J. Hydrol.*, **1994**, 161, 327-346. [https://doi.org/10.1016/0022-1694\(94\)90133-3](https://doi.org/10.1016/0022-1694(94)90133-3)

3. Skoog, D.A.; West, D.M., *Fundamentals of Analytical Chemistry*, 9 ed.; Cengage: Independence, KY, 2014.
4. deLevie, R. *How to Use Excel in Analytical Chemistry and in General Scientific Data Analysis*; Cambridge University Press, UK, 2004.
5. Butler, J. N. *Ionic Equilibrium*; Wiley: New York, 1998.
6. Lehninger, A.L.; Nelson, D.L. *Lehninger's Principles of Biochemistry*, 6 ed.; W.H. Freeman: New York, 2013.
7. J.M. Tymoczko, J.L.; Stryer, L. *Biochemistry*, 8 ed.; W.H. Freeman: New York, 2002.
8. Legarra, M.; Blitz, A.; Czegeny, Z.; Antal, M. J. Aqueous Potassium Bicarbonate/Carbonate Ionic Equilibria at Elevated Pressures and Temperatures, *Ind. Eng. Chem. Res.*, **2013**, 52, 13241– 13251.
<https://doi.org/10.1021/ie070819m>
9. Stumm, W.; Morgan, J. J. *Aquatic Chemistry*, 3ed.; Wiley: New York, 1995.
10. Laterza, O.F.; Hansen, W. R.; Taylor, L.; Curthoys, N. P. Identification of an mRNA-Binding Protein and the Specific Elements That May Mediate the pH-Responsive Induction of Renal Glutaminase mRNA. *J Biol. Chem.* **1997**, 272, 22481–22488. <https://doi/10.1074/jbc.272.36.22481>
11. Tooke, D.L.; Smith, G.C.; Griffin, L.R. Dispersion of Hydrogen Sulfide from Wastewater Lagoons at a Kraft Pulp Mill. In *Proceedings of the 2003 TAPPI International Environmental Conference*, D. Edelman, ed.; TAPPI: Norcross, GA, 2003.
12. Smith, G. C.; Hossain, Md. M.; MacCarthy, P. 3-D Surface Visualization of pH Titration “Topos”: Equivalence Point Cliffs, Dilution Ramps, and Buffer Plateaus. *J. Chem. Educ.*, **2014**, 91 (2), 225–231.
<https://doi.org/10.1021/ed400297t>
13. Smith, G. C. and Hossian, Md M. 3-D Visualization of Buffer Capacity Topos: Buffer Ridges, Equivalence Point Canyons and Dilution Ramps. *J. Chem. Educ.*, **2016**, 93 (1), 122–130.
<http://pubs.acs.org/doi/abs/10.1021/acs.jchemed.5b00439>
14. Sorensen, S. P. L. Über die Messung und die Bedeutung der Wasserstoffionenkonzentration bei Enzymatischen Prozessen. *Biochem. Zeitschr.*, **1909**, 21: 131–304.
15. Sillen, L.G.; Lange, P.W.; Gabrielson, C.O. *Problems in Physical Chemistry*; Prentice-Hall: New York, 1952.
16. Sillen, L.G. Graphical Presentation of Equilibrium Data. In *Treatise on Analytical Chemistry*, Kolthoff, I.M.; Elving, P.J.; Interscience: New York, 1959.

17. McMasters, D.L.; Schaap, W.B. High-Speed Calculation of Least-Squares Best Consecutive Formation Constants of Metal-Ion Complexes Using the Electronic Computer. *Proc. Indiana Acad. Sci.*, **1958**, 67, 111-116.
18. Garrels, R.M., Thompson, M.E. A Chemical Model for Sea Water at 25°C and One Atmosphere Total Pressure. *Am. J. Sci.*, **1962**, 260, 57-66.
<https://doi.org/10.2475/ajs.260.1.57>
19. Perrin, D.D.; Sayce, I.G. Computer Calculation of Equilibrium Concentrations in Mixtures of Metal Ions and Complexing Species, *Talanta*, **1967**, 14 (7), 833-842. [https://doi.org/10.1016/0039-9140\(68\)80200-0](https://doi.org/10.1016/0039-9140(68)80200-0)
20. Ramette, R. W. The Acid-Base Package: A Collection of Useful Programs for Proton Transfer Systems. *J. Chem. Educ. Software* **1989**, 2B, No. 2.
21. Ramette, R. W. Buffers Plus. *J. Chem. Educ.* **1998**, 75 (11) 1504.
<https://pubs.acs.org/doi/pdf/10.1021/ed075p1504>
22. Gutz, I. G. R. CurTiPot <http://www2.iq.usp.br/docente/gutz/Curtipot.html> (accessed February 2017).
23. Martell, A.E.; Smith, R.M. *Critical Stability Constants*; Plenum Press: New York, 1974-1989, 6 volumes.